Supporting Information

Remarkable Enhancement in Hydrogenation Ability by Phosphidation of Ruthenium: Specific Surface Structure Having Unique Ru Ensembles

Shinya Furukawa,*[,†,¶] Yukihiko Matsunami,[‡] Ikutaro Hamada,[‖,§,¶] Yasushi Hashimoto,[#] Yasushi Sato,[#] Takayuki Komatsu*[,‡]

[†] *Institute for catalysis, Hokkaido University, N21, W10, Kita-ku, Sapporo, Japan, 001-0021*

[¶] *Element Strategy Initiative for Catalysis and Battery, Kyoto University, Kyoto Daigaku Katsura, Nishikyo-ku, Kyoto, Japan, 615-8510*

[‡] *Department of Chemistry, School of Science, Tokyo Institute of Technology, 2-12-1, Meguro-ku, Tokyo, Japan, 152-8550*

[‖] *Department of Precision Science & Technology, Graduate School of Engineering, Osaka University, 2-1 Yamada-oka, Suita, Osaka, Japan 565-0871*

[§] *Global Research Center for Environment and Energy based on Nanomaterials Science, Naitonal Institute for Materials Science, 1-1 Namiki, Japan, 305-0044*

[#] *Central Technical Research Laboratory, JXTG Nippon Oil & Energy Co., 8 Chidoricho, Naka-ku, Yokohama, Japan, 231-0815*

E-mail: furukawa@cat.hokudai.ac.jp,

Tel: +81-11-706-9162, Fax: +81-11-706-9163

E-mail: komatsu.t.ad@m.titech.ac.jp,

Tel: +81-3-5734-3532, Fax: +81-3-5734-2758

Experimental Section

Catalyst preparation

A series of monometallic catalysts were prepared by pore-filling impregnation using silica as a support (M/SiO_2, M = Pt, Ir, Pd, Rh, Ru, Ni, and Co; M loading, 3 wt%). Aqueous solution of H_2PtCl_6 (Furuya Kinzoku, Pt: 8.71 wt%), $(NH_4)_2IrCl_6$ (Strem Chemicals, 99%), $Pd(NO_3)_2$ (Furuya Kinzoku, Pd: 4.63 wt%), $Rh(NO_3)_3$ (Furuya Kinzoku, Pt: 4.53 wt%), $Ru(NO_3)_3$ (Furuya Kinzoku, Pt: 4.57 wt%), $Ni(NO_3)_2{\cdot}6H_2O$ (Kanto, 99%), or $Co(NO_3)_2{\cdot}6H_2O$ (Kanto, 98%) was added to dried silica gel (CARiACT G-6, Fuji Silysia, S_{BET} = 470 $m^2\ g^{-1}$) so that the solutions filled the silica pores (pore volume: 0.76 $cm^3 g^{-1}$, metal concentration: 185 mM for the synthesis of Rh/SiO_2). The mixtures were sealed overnight at room temperature and dried over a hot plate, followed by calcination at 673 K in the air for 1 h and the subsequent reduction under flowing H_2 (Taiyo Nissan, 99.99999%) at 673 K for 1 h. The calcination procedure was skipped for Pt, Pd, Rh, and Ni. Silica-supported metal phosphide catalysts (M_xP_x/SiO_2, M = Pt, Ir, Pd, Rh, Ru, Ni, and Co; M loading, 3 wt%) were prepared by successive impregnation of phosphorus to M/SiO_2. Aqueous solutions of $(NH_4)_2HPO_4$ (Kanto, 99%) was added to the reduced M/SiO_2 in a similar fashion mentioned above. For Ir and Pd, acetone solution of triphenylphosphine (PPh_3) instead of the aqueous solution of $(NH_4)_2HPO_4$ was added to unreduced (just calcined) M/SiO_2. The P/M ratio was adjusted to 1 (Ir, Pd, Rh, and Ru) or 2 (Pt, Ni, and Co). The as-impregnated catalyst was then dried and reduced at 873 K for 1 h. Ru_2P catalysts using other supports (Table S1) were prepared by a conventional impregnation method using an excess amount of water. Aqueous solution of $Ru(NO_3)_3$ was added dropwise to the vigorously stirred support dispersed in water (30ml), followed by stirring overnight at room temperature. The mixture was then dried and reduced at 673 K for 1 h. Successive impregnation of Phosphorous was done in the similar manner using aqueous solutions of $(NH_4)_2HPO_4$, followed by reduction at 873 K for 1 h.

Characterizations

The crystal structure of the prepared catalyst was examined by powder X-ray diffraction with a Rigaku SmartLab using an X-ray source of Cu Kα. Transmission electron microscopy (TEM) was conducted using a JEOL JEM-2010F microscope at an accelerating voltage of 200 kV. To prepare the TEM specimen, the sample was sonicated in ethanol and then dispersed on a Cu grid supported by an ultrathin carbon film. Fourier-transformed infrared (FT-IR) spectra of adsorbed CO and toluene were obtained with a JASCO FT/IR-430 spectrometer in transmission mode. A self-supporting wafer (50 mg cm^{-2}) of catalyst was placed in a quartz cell with CaF_2 windows and attached to a glass circulation system. The catalyst was reduced under flowing H_2 at 473 K for 0.5 h, evacuated at the

same temperature for 5 min, and cooled to room temperature. After the pretreatment, a spectrum was recorded as the base line for subsequent measurements. For CO adsorption, a pulse of CO, typically of 10^1–10^3 Pa order, was introduced in a stepwise manner at room temperature. For toluene adsorption and desorption, toluene (3.0 kPa) was introduced to the catalysts and evacuated at room temperature until no spectral changed was observed. Then, the catalyst was heated under vacuum with a ramping rate of 10 $Kmin^{-1}$ up to 473 K. All spectra were recorded at 1 cm^{-1} resolution. Metal dispersion was estimated by CO chemisorption using a glass circulation system equipped with a U-tube oil manometer. The catalyst in quartz tube reactor was reduced by H_2 at 473 K for 0.5 h, followed by evacuation at the same temperature. After cooling to room temperature, the reactor was connected to the manometer, followed by exposing to CO. The amount of chemisorbed CO was measured by manometry. TG-DTA study of the fresh and spent catalysts were carried out under an oxidative atmosphere (250 ml/min of air) with SII TG/DTA7200 analyzers using 10 mg of sample and a 10 °C/min temperature increase rate up to 800°C.

Reaction condition

Toluene hydrogenation was carried out in a fixed-bed continuous flow system using a quartz tube reactor (internal diameter: 7 mm) under an atmospheric pressure. The catalyst (0.17 g) was reduced prior to the reaction under H_2 flow (6 $mlmin^{-1}$) at 473 K for 0.5 h. After the reduction, the reactor was purged by N_2 (6 $mlmin^{-1}$) at the same temperature. The reaction was initiated by feeding the reaction mixture (toluene, H_2, and N_2 with a molar ratio of 1:7.5:7.5) at 473 K. Toluene was fed using a micro feeder equipped with a stainless cannula of which edge was located just above the catalyst bed. The products were trapped by an ice trap downstream and analyzed by flame ionization detector gas chromatography (FID-GC) equipped with a CP-Silica PLOT column (VARIAN, 0.32 mmφ×30 m). Toluene conversion (C_{tol}) and methylcyclohexane selectivity (S_{MCH}) were estimated by the following equation: $C_{tol} = (n_{MCH} + n_B) / (n_T + n_{MCH} + n_B) \times 100$ (%), $S_{MCH} = n_{MCH} / (n_{MCH} + n_B) \times 100$ (%), where, n_T, n_{MCH}, and n_B are mole of toluene, methylcyclohexane, and benzene as a by-product, respectively.

Computational Details

All the density functional theory calculations were performed by using the projector augmented wave (PAW) method[1] as implemented in the Quantum ESPRESSO code.[2] We used the rev-vdW-DF2 functional,[3] which has been shown to describe the physisorption as well as chemisorption systems accurately. We used an efficient algorithm[4] of the self-consistent van der Waals density functional[5,6] implemented[7] in Quantum-ESPRESSO. The PAW potentials from pslibrary 1.0.0[8] were used to describe the electron-ion interaction, and the wave functions and the augmented charge density were expanded in terms of a plane-wave basis with the kinetic cutoff energy of 80 and 640 Ry, respectively. We used the PAW potentials generated using the Perdew-Burk-Ernzerhof (PBE) functional,[9] and the use of PBE potentials in vdW-DF calculations was validated in ref 10. The structures of bulk Ru and Ru_2P were optimized using Γ-centered 12×12×12 *k*-point set and 4×4×4 Monkhorst-Pack[11] *k*-point set, respectively. Optimized lattice parameters are a=2.706 Å and c=4.278 Å for Ru in the hexagonal closed pack structure and a=5.864 Å, b=3.873 Å, and c=6.980 Å for Ru_2P, respectively, which are in good agreement with the experimental values.[12,13]

The surfaces were modeled by slab models constructed using the theoretically optimized lattice parameters, and we used (3×3) 5-layer slab and (1×2) 4-layer slab for Ru(0001) and Ru_2P(112), respectively, and 4×4 Γ-centered *k*-point set and 4×4 Monkhorst-Pack *k*-point set were used to sample the surface Brillouin zone. The slabs were separated by a vacuum equivalent to 6 monolayer thickness (~15 Å) for Ru and ~13 Å for Ru_2P. The Hermite-Gaussian function of the order 1 with the smearing width of 0.01 Ry was used to treat the Fermi surface.[14] Adsorbates were put on one side of the slab, and the spurious electrostatic interaction between the neighboring slabs were eliminated by using the Green's function technique.[15,16] The two bottommost layers were fixed to their respective bulk positions, and the remaining degrees were relaxed until the maximum force drops below 5.1 × 10^{-3} eV/Å (1×10^{-4} Hartree/Bohr). The adsorption energy was defined by $E_{\mathrm{ads}} = -[E_{\mathrm{tot}} - E_{\mathrm{tot}}^{\mathrm{mol}} - E_{\mathrm{tot}}^{\mathrm{sub}}]$, where E_{tot}, $E_{\mathrm{tot}}^{\mathrm{mol}}$, and $E_{\mathrm{tot}}^{\mathrm{sub}}$ are total energies of combined system, adsorbate, and substrate, respectively.

For the surface energy calculations, we constructed symmetric slabs using the theoretically optimized lattice parameters, which contain 6 atomic layers and are separated by a vacuum of ca 10 Å. Γ-centered 4×4, 4×4, 4×2, 4×4, 4×4, 4×8, 4×4, and 2×8 *k*-point meshes were used for (210), (112), (013), (111), (020), (301), (211), and (103) surfaces, respectively. Atoms in the slabs were fully relaxed.

Tables

Table S1. Catalytic performances of Ru_2P catalysts using various supports in toluene hydrogenation.

support	product name	S_{BET} / m^2g^{-1}	Conv. (%)	Sel. (%)
active carbon	DARCO	674	14.8	100
Al_2O_3	JRC-ALO-8	178	43.7	99.1
CeO_2	JRC-CEO-1	157	14.7	99.7
MgO	JRC-MGO-4	33	21.6	99.3
TiO_2	JRC-TIO-6 (rutile)	100	42.1	99.7
SiO_2	CARiACT G6	470	48.7	100

Table S2. Calculated surface energies of various planes of Ru_2P.

Surface	Surface energy (J/m^2)
(210)	2.05
(112)	2.21
(013)	2.38
(111)	2.43
(020)	2.43
(301)	2.45
(211)	2.52
(103)	2.57

Figures

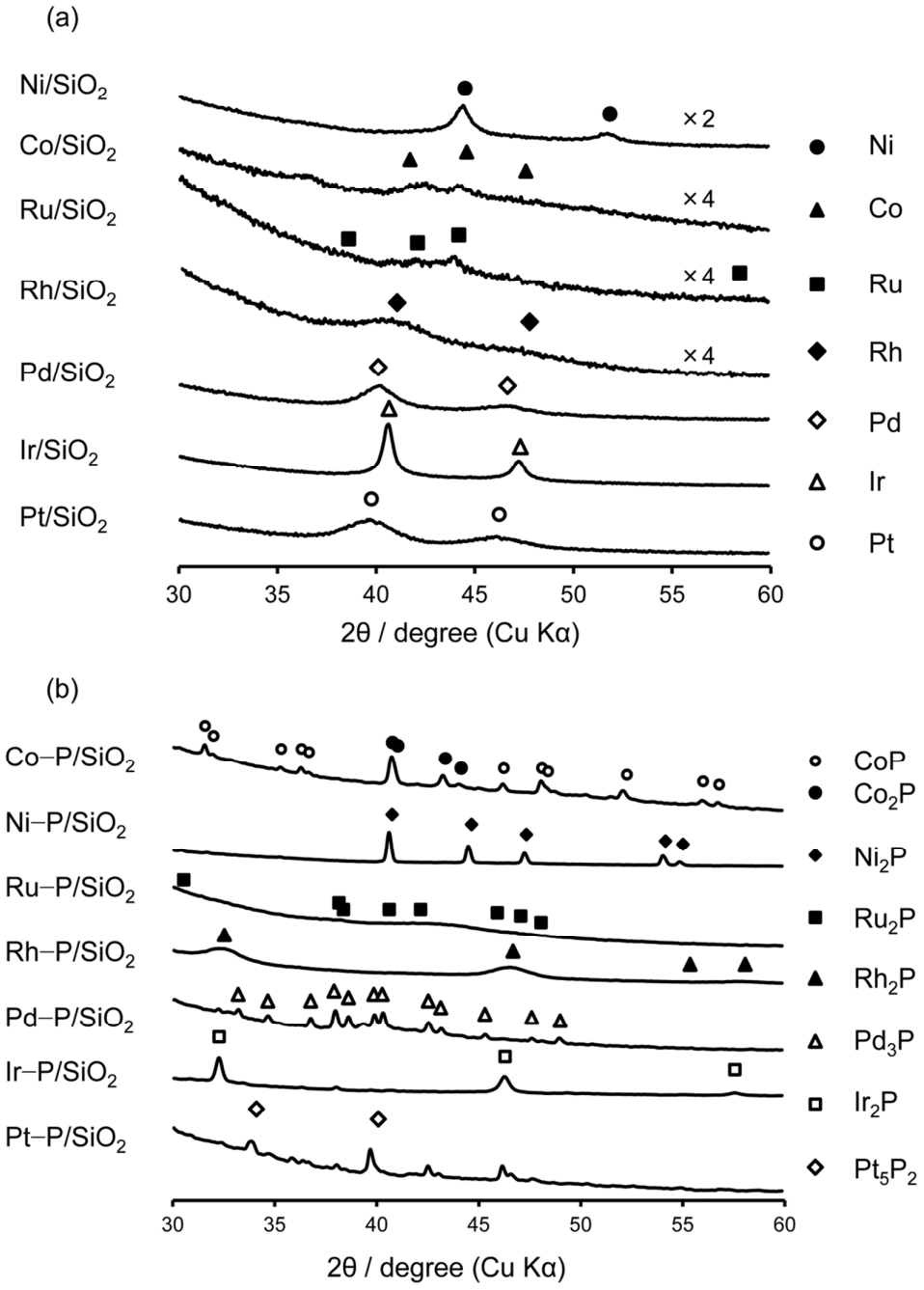

Figure S1. XRD patterns of silica-supported (a) monometallic and (b) metal-phosphide catalysts.

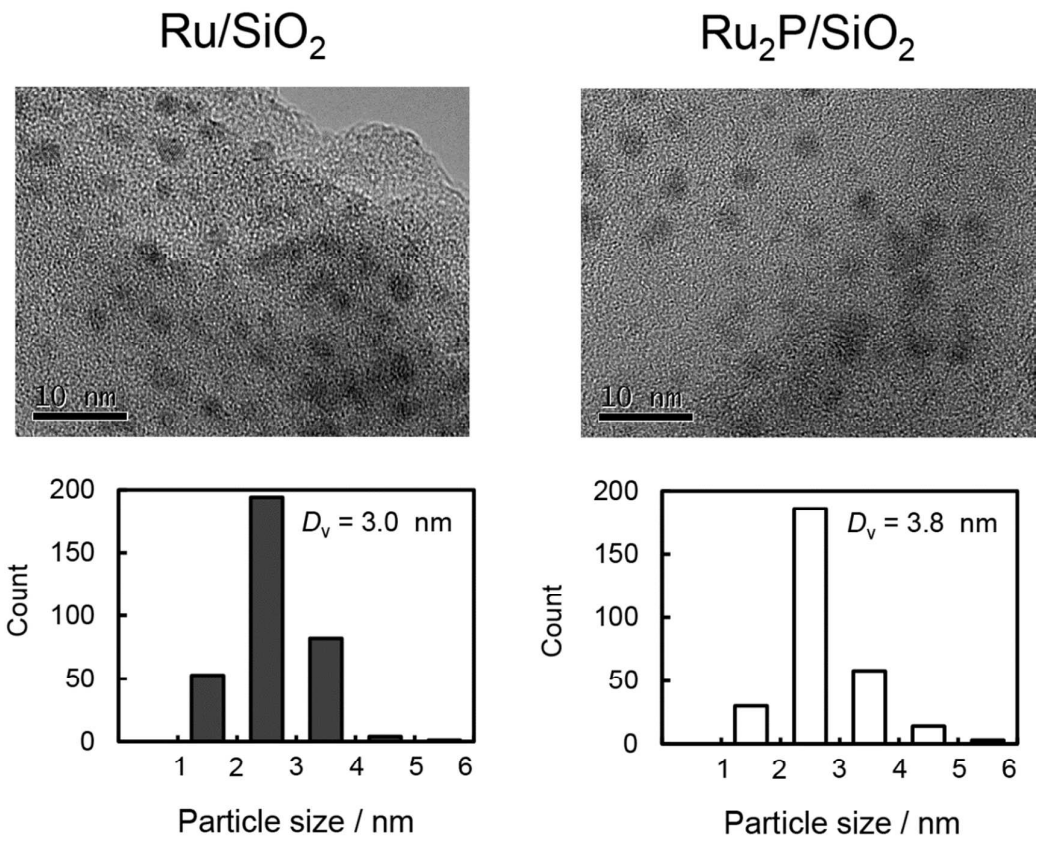

Figure S2. TEM image and size distribution of Ru/SiO_2 (left) and Ru_2P/SiO_2 (right). D_v indicates volume-weighted mean diameter.

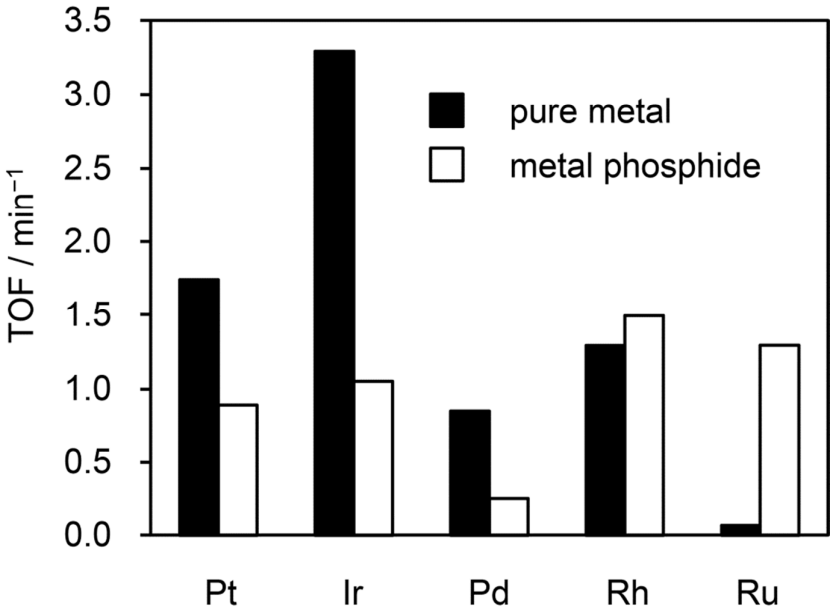

Figure S3. TOF of tested catalysts in toluene hydrogenation.

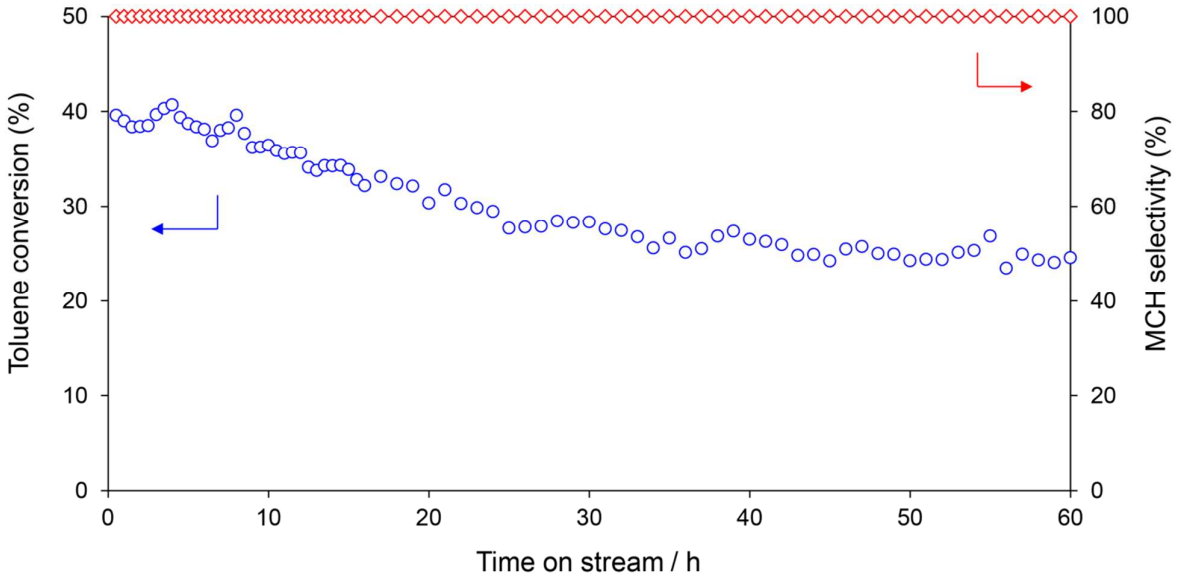

Figure S4. Change in the catalytic performance of Ru_2P/SiO_2 in toluene hydrogenation.

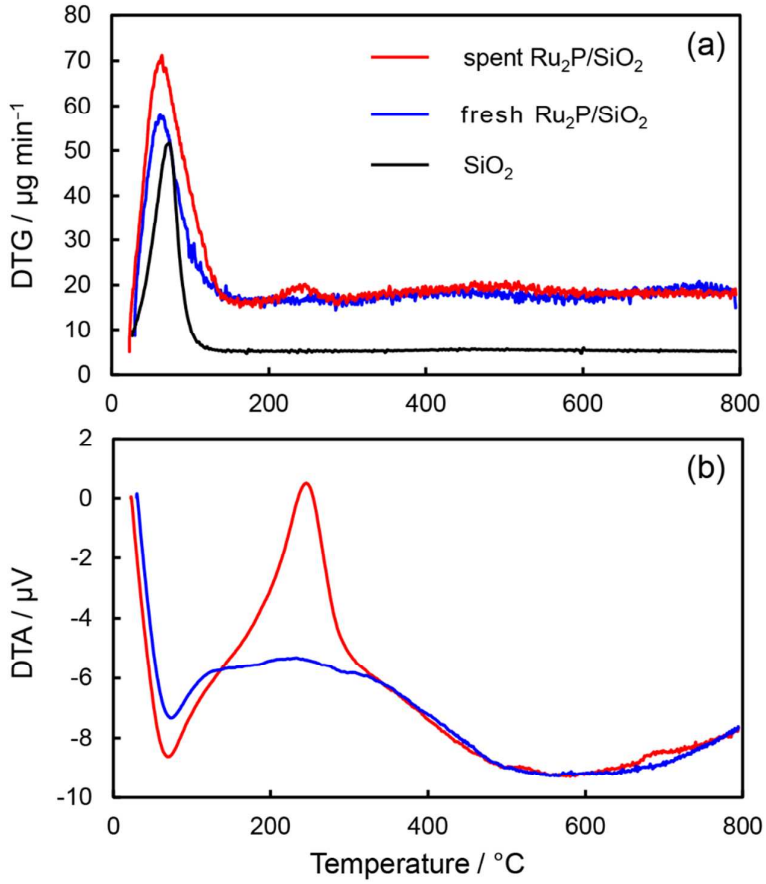

Figure S5. (a) DTG and (b) DTA profiles of fresh and spent Ru_2P/SiO_2. For spent catalyst, Ru_2P/SiO_2 after 60 h of toluene hydrogenation was used. The strong DTG peak below 100°C corresponds to water desorption. The exothermic peak at 240°C indicates combustion of carbonaceous deposit.

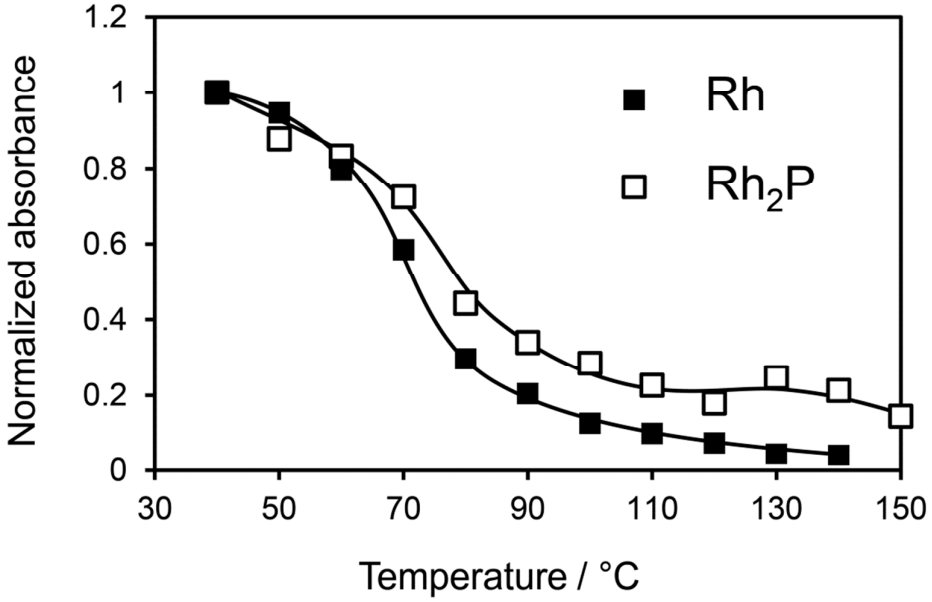

Figure S6. TPD profiles (ca. 3530 cm^{-1}) of toluene desorption for Rh-based catalysts.

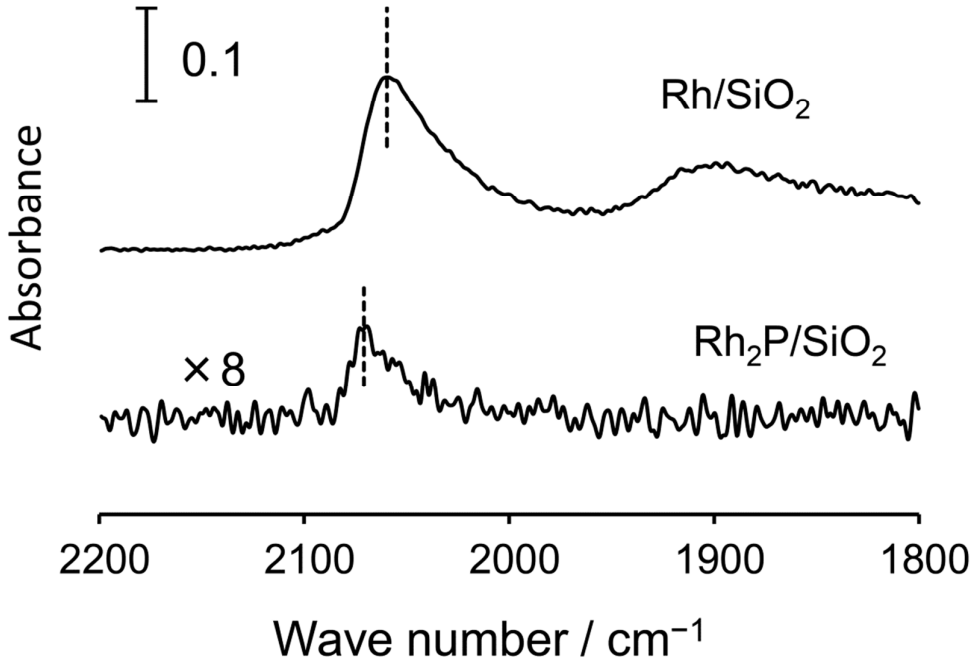

Figure S7. FT-IR spectra of CO adsorbed on Rh-based catalysts.

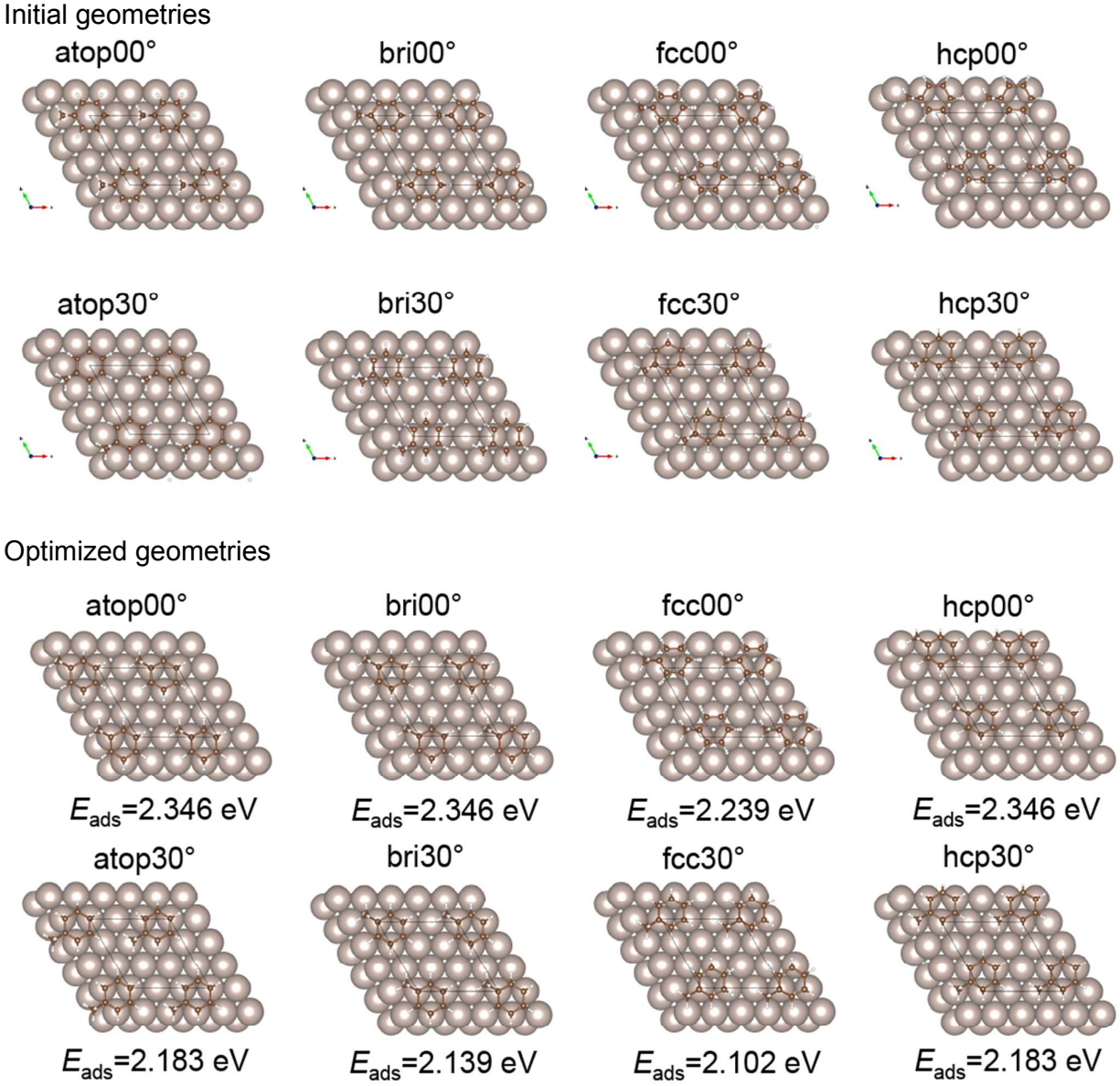

Figure S8a. Geometry optimization for toluene adsorbed on Ru(0001) surface. Gray: Ru, brawn: C, white: H. For the most stable adsorption geometry, aromatic C atoms at 1, 3, and 5 positions bind to Ru with σ-like coordination and with the methyl group pointing toward another hollow site (two C-H bonds directed to Ru atoms).

Conformation 1: E_{ads} = 2.708 eV

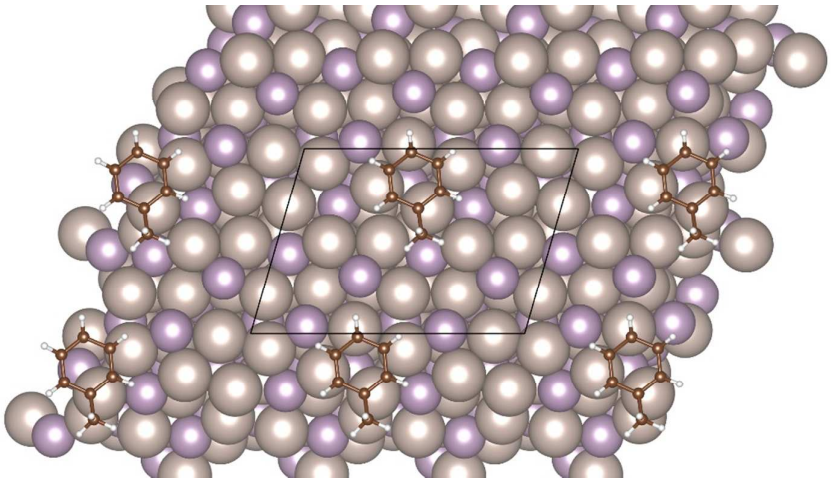

Conformation 2: E_{ads} = 2.768 eV

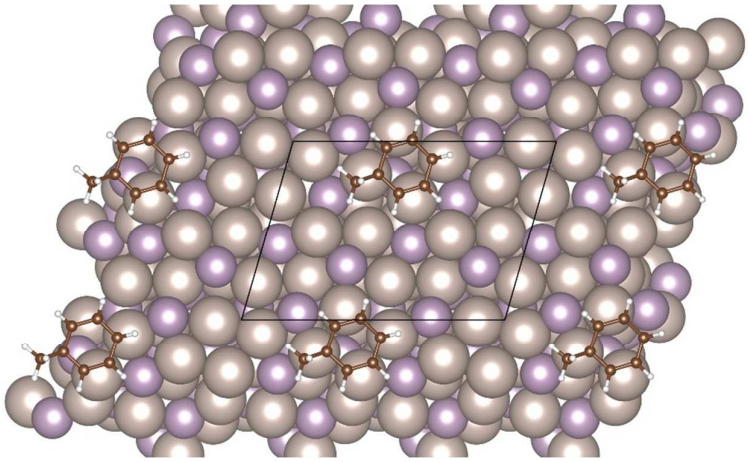

Conformation 3: E_{ads} = 2.712 eV

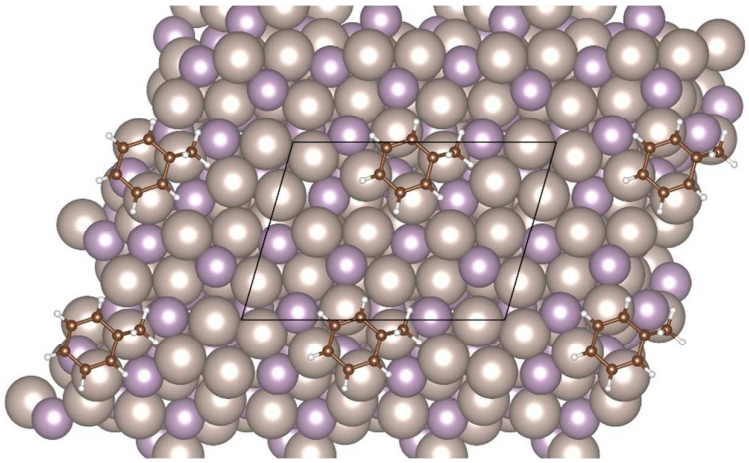

Figure S8b. Optimized geometries of toluene adsorbed on $Ru_2P(112)$ surface. Gray: Ru, purple: P brawn: C, white: H.

Close-up of the toluene conformation (Figure S8b)

Conformation 1

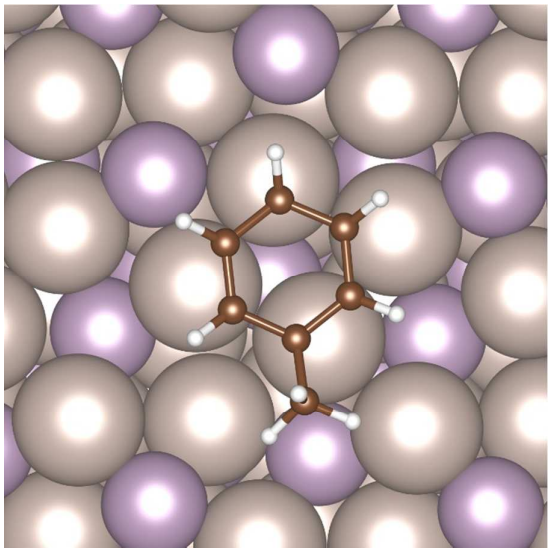

Conformation 2

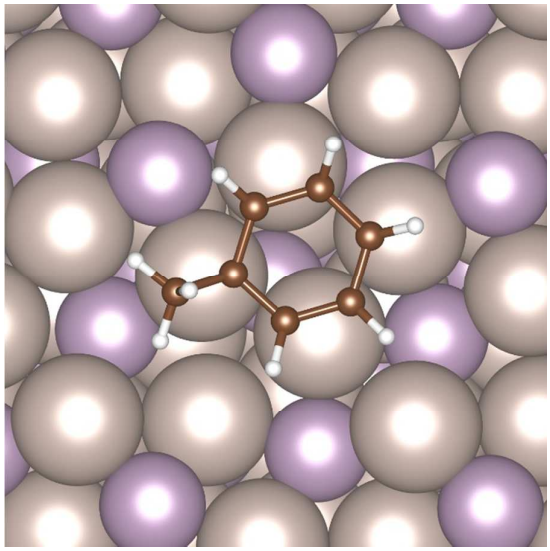

Conformation 3

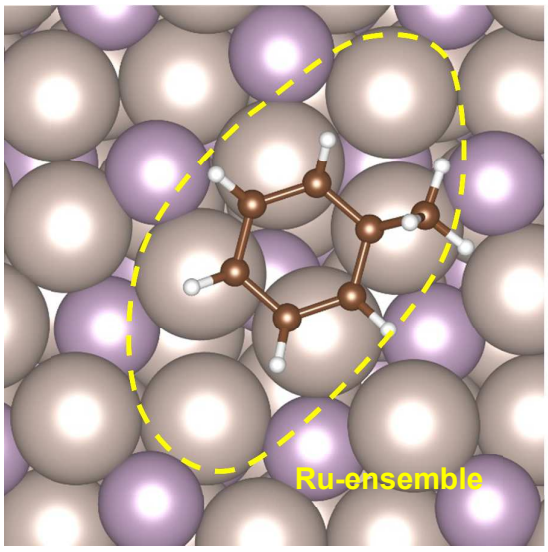

(a) 2 toluene on 2 Ru-ensemble (optimized)

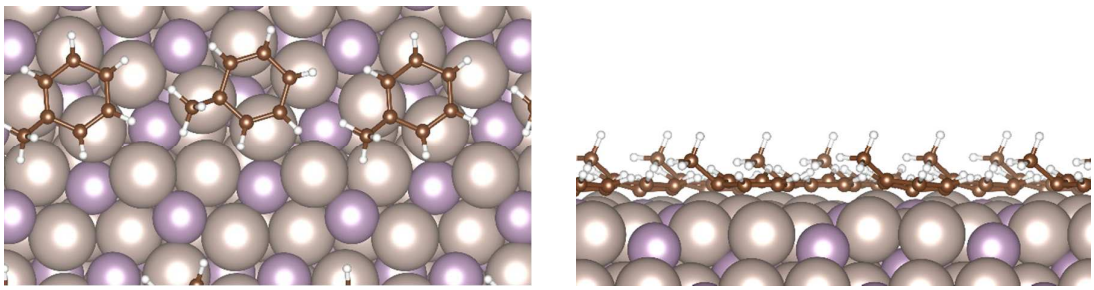

(b) 1 toluene on 1 Ru-ensemble and 1 toluene on 1 H-adsorption site (initial)

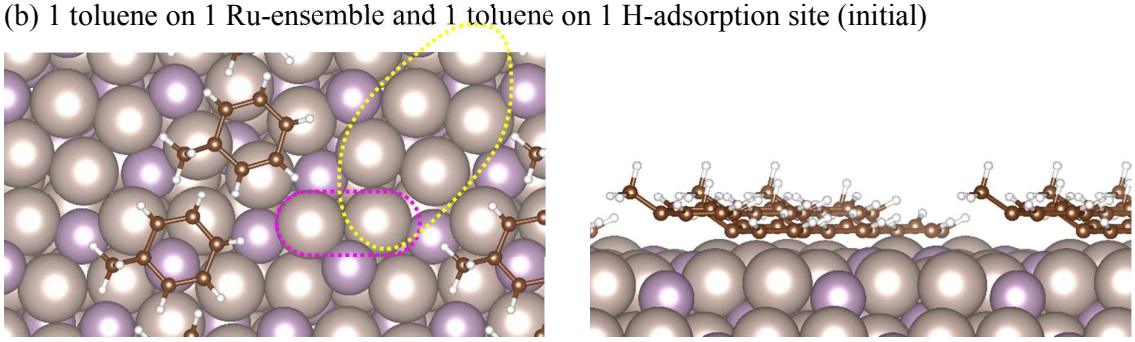

(c) 2 toluene on 2 Ru-ensemble and 1 toluene on 1 H-adsorption site (initial)

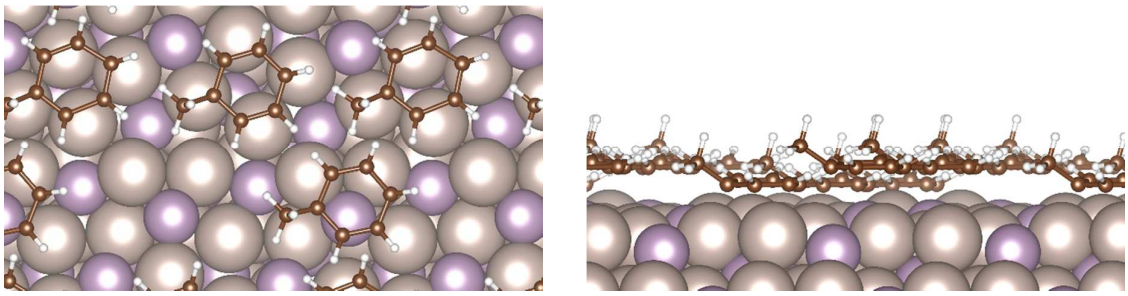

(d) 2 toluene on 2 Ru-ensemble and 2 toluene on 2 H-adsorption site (full coverage) (initial)

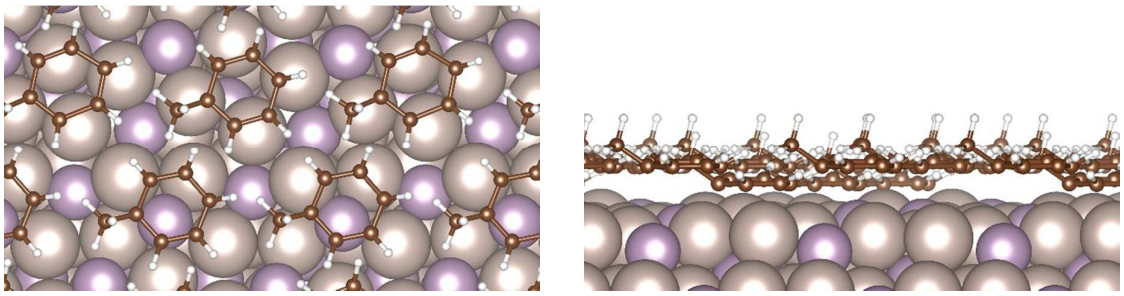

Figure S9. Optimized and initial structures of toluene adsorbed on $Ru_2P(112)$ surface at high coverages. Yellow and purple dotted lines indicate Ru-ensemble and H-adsorption sites, respectively. Geometry optimization of the structures (b), (c), and (d) did not converged.

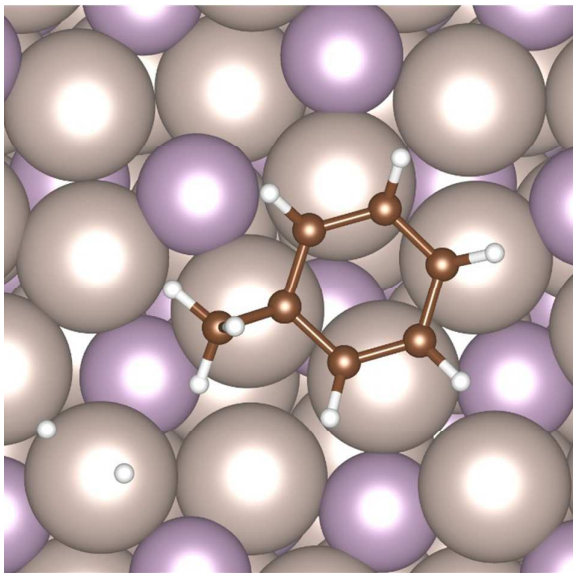

toluene (conformation 1) + 2H
E_{ads} (2H) = 0.69 eV

Figure S10. Optimized structure of dissociated two H atoms from one H_2 molecule at an H-adsorption site on $Ru_2P(112)$ surface. The adsorption energy was defined by $E_{\mathrm{ads}} = -[E_{\mathrm{tot}} - E_{\mathrm{tot}}^{\mathrm{mol}} - E_{\mathrm{tot}}^{\mathrm{sub}}]$, where E_{tot}, $E_{\mathrm{tot}}^{\mathrm{mol}}$, and $E_{\mathrm{tot}}^{\mathrm{sub}}$ are total energies of combined system, H_2, and toluene adsorbed Ru_2P substrate, respectively.

References

(1) Blöchl, P. E. Projector augmented-wave method. *Phys. Rev. B: Condens. Matter Mater. Phys.* **1994**, *50*, 17953–17979.

(2) Giannozzi, P.; Baroni, S.; Bonini, N.; Calandra, M.; Car, R.; Cavazzoni, C.; Ceresoli, D.; Chiarotti, G. L.; Cococcioni, M.; Dabo, I.; Dal Corso, A.; de Gironcoli, S.; Fabris, S.; Fratesi, G.; Gebauer, R.; Gerstmann, U.; Gougoussis, C.; Kokalj, A.; Lazzeri, M.; Martin-Samos, L.; Marzari, N.; Mauri, F.; Mazzarello, R.; Paolini, S.; Pasquarello, A.; Paulatto, L.; Sbraccia, C.; Scandolo, S.; Sclauzero, G.; Seitsonen, A. P.; Smogunov, A.; Umari, P.; Wentzcovitch, R. M. QUANTUM ESPRESSO: a modular and open-source software project for quantum simulations of materials. *J. Phys.: Condens. Matter* **2009**, *21*, 395502–395519.

(3) Hamada, I. van der Waals density functional made accurate. *Phys. Rev. B: Condens. Matter Mater. Phys.* **2014**, *89*, 121103.

(4) Román-Pérez, G.; Soler, Efficient Implementation of a van der Waals Density Functional: Application to Double-Wall Carbon Nanotubes. J. M. *Phys. Rev. Lett.* **2009**, *103*, 096102.

(5) Dion, M.; Rydberg, H.; Schröder, E.; Langreth, D. C.; Lundqvist, B. I. Van der Waals Density Functional for General Geometries. *Phys. Rev. Lett.* **2004**, *92*, 246401.

(6) Berland, K.; Cooper, V. R.; Lee, K.; Schröder, E.; Thonhauser, T.; Hyldgaard, P.; Lundqvist, B. I. van der Waals forces in density functional theory: a review of the vdW-DF method. *Rep. Prog. Phys.* **2015**, *78*, 066501.

(7) Thonhauser, T.; Cooper, V. R.; Li, S.; Puzder, A.; Hyldgaard, P.; Langreth, D. C. Van der Waals density functional: Self-consistent potential and the nature of the van der Waals bond. *Phys. Rev. B:*

Condens. Matter Mater. Phys. **2007**, *76*, 125112.
(8) Dal Corso, A. Pseudopotentials periodic table: From H to Pu. *Comput. Mater. Sci.* **2014**, *95*, 337–350.
(9) Perdew, J. P.; Burke, K.; Ernzerhof, M. Generalized Gradient Approximation Made Simple. *Phys. Rev. Lett.* **1996**, *77*, 3865–3868.
(10) Callsen, M.; Hamada, I. Assessing the accuracy of the van der Waals density functionals for rare-gas and small molecular systems. *Phys. Rev. B: Condens. Matter Mater. Phys.* **2015**, *91*, 195103.
(11) Monkhorst, H. J.; Pack, J. D. Special points for Brillouin-zone integrations. *Phys. Rev. B* **1976**, *13*, 5188–5192.
(12) Arblaster, J. W. Crystallographic Properties of Ruthenium. *Platinum Met. Rev.* **2013**, *57*, 127–136.
(13) Rundqvist, S. Phosphides of the Platinum Metals. *Nature* **1960**, *185*, 31–32.
(14) Methfessel, M.; Paxton, A. T. High-precision sampling for Brillouin-zone integration in metals. *Phys. Rev. B: Condens. Matter Mater. Phys.* **1989**, *40*, 3616–3621.
(15) Otani, M.; Sugino, O. First-principles calculations of charged surfaces and interfaces: A plane-wave nonrepeated slab approach. *Phys. Rev. B: Condens. Matter Mater. Phys.* **2006**, *73*, 115407.
(16) Hamada, I.; Otani, M.; Sugino, O.; Morikawa, Y. Green's function method for elimination of the spurious multipole interaction in the surface/interface slab model. *Phys. Rev. B: Condens. Matter Mater. Phys.* **2009**, *80*, 165411.